Morphological variation of multiwall carbon nanotubes in supercritical water oxidation

Jia-Yaw Chang, Bertrand Lo, Meili Jeng, Shin-Hwa Tzing, and Yong-Chien Ling[a)]
Department of Chemistry, National Tsing Hua University, Hsinchu, Taiwan 30013, Republic of China

(Received 5 March 2004; accepted 29 July 2004)

Multiwall carbon nanotubes (MWNTs) with different morphology were prepared using supercritical water (SCW) oxidation and investigated by transmission electron microscope (TEM) and electron energy-loss spectroscopy (EELS). TEM results indicate that the peeling and sharpening of MWNTs are influenced by the etching process in SCW oxidation, of which oxidation time and amount of oxygen used is crucial. A simplified etching model is proposed, which indicates that the difference of mean etching rate between two adjoining blocks causes the morphological variation of MWNTs. The EELS results show change in characteristic energy-loss peaks as a function of total shell numbers along longitudinal axis of individual peeled tube. © *2004 American Institute of Physics*. [DOI: 10.1063/1.1798393]

Multiwall carbon nanotubes (MWNTs)[1] are carbon nanotubes (CNTs) composed of a series of coaxial cylindrical shells (CSs), each CS has different graphene structure depending on the helicity and the diameter of the cylinder.[2] The property of each CS plays an important role on morphological variation of MWNTs. For example, Cumings *et al.*[3] used electrically driven vaporization to remove successive outer CSs of MWNTs. Collins *et al.*[4] used current-induced electrical breakdown for stepwise removal of outer CSs of MWNTs as each layer has different electronic structure. Armchair CNTs have several precursor states which might delay O_2 adsorption at the armchair edge,[5] which enables selective etching between armchair and zigzag tubes by controlling the etching time. Understanding the morphological variation of MWNTs is crucial for the design and performance of nanodevices. Several techniques have been applied for opening and etching of CNTs, including heat treatment in O_2,[6] air,[7] CO_2,[8] reflux in HNO_3,[9] plasma etching,[10,11] and supercritical water (SCW).[12–16] However, detailed study of morphological variation of MWNTs under these drastic oxidation conditions is limited. The aim of the present work is to study the mechanism of morphological variation of MWNTs in SCW oxidation. The concept of axial etching rates and iso-etching blocks of CSs are introduced to explain the morphological variation. Further, electron energy-loss spectroscopy (EELS)[17–19] was used to show the peak shifts as a function of number of layers along longitude axis of a peeled tube.

The MWNTs were prepared by electric-arc discharge method.[20] An aliquot of 20 mg of crude MWNTs were loaded into the reaction cell and followed by introducing oxygen gas (~2 or 4 mmol) into reaction cell. A high-pressure liquid chromatograph pump was used to pump deionized water into reaction cell at the desired temperature (400 or 600 °C) until 27.5 MPa operating pressure was attained. The reaction proceeded for 20, 60, and 120 min, respectively. After each experiment, the reaction cell was cooled to room temperature and MWNTs were collected in a beaker, dispersed in methanol with an ultrasonic bath. The suspensions were then dropped onto Cu grids coated with lacey carbon films. The characterization of the ultrastructure and the EELS measurement of MWNTs were carried out using a transmission electron microscope (TEM, Philips, Tecnai 20) with a LaB_6 type filament at an operating voltage of 200 kV.[15]

TEM images show peeling and sharpening of MWNTs at different stages of oxidation in SCW and the etching sites [arrow marks in Figs. 1(a)–1(e)]. The process starts with the outmost end-cap of tube being stripped-off, SCW and O_2 attacking on successive end-caps of inner tubes, followed by

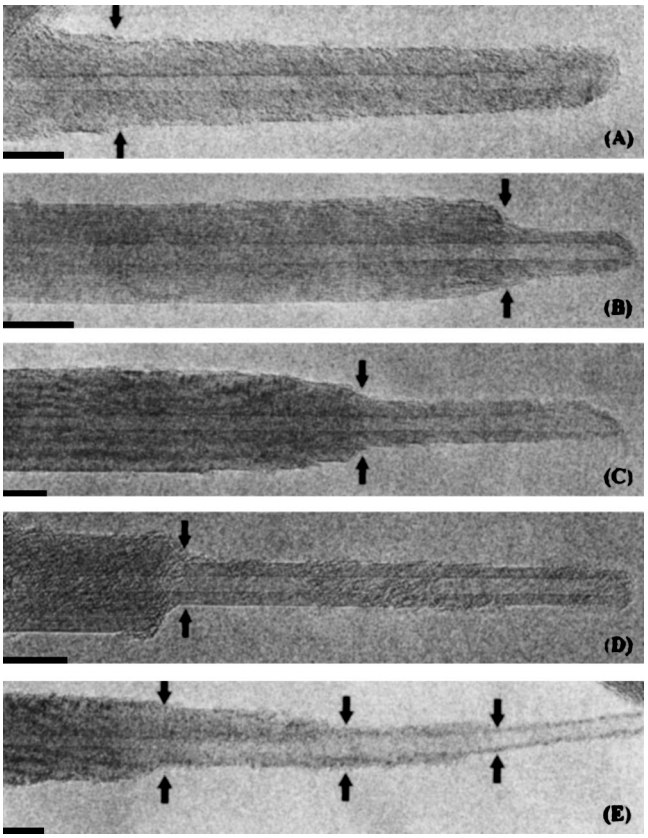

FIG. 1. TEM images of MWNTs in SCW oxidation at 27.5 MPa. (a) 60 min, 400 °C, and ~2 mmol O_2, (b) 20 min, 400 °C, and ~2 mmol O_2, (c) and (d) 60 min, 400 °C, and ~2 mmol O_2, (e) 120 min, 600 °C, and ~4 mmol O_2. The scale bar has a length of 10 nm.

[a)]Electronic mail: ycling@mx.nthu.edu.tw

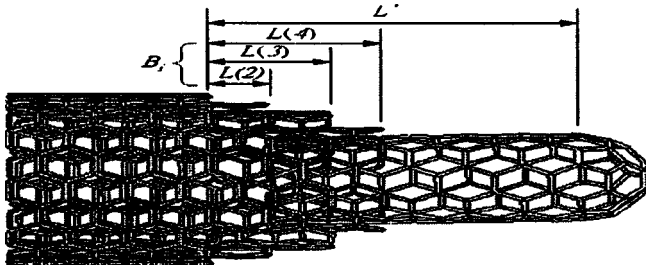

FIG. 2. The geometry of peeled tube [L' designates the axial etching of outmost cylindrical shell; $L(2)$, $L(3)$, and $L(4)$ are the residual length of axial etching belong to the same block, B_j].

etching of consecutive inner shells. Different morphology of MWNTs are observed [Figs. 1(a)–1(d)]. To understand the morphological variation of MWNTs and to simplify the description of MWNTs etching process, we assume (1) the peeled tubes are the consequences of the etching of a series of coaxial CSs, (2) the intrinsic character of each CS dominates the axial etching rate [$v_{\text{A.E.}}(i)$ for ith shell] of peeled tubes, (3) successive coaxial CSs with similar properties and etching rates are defined as iso-etching blocks (B), and (4) the etching in the circumferential edge of each CS occurs only after the end-cap in each CS being removed. Figure 2 depicts the geometry of the peeled tubes used for the proposed model. Lateral shell number, $i=1,2,\ldots,n$, is designated from the outer to inner CS. The residual length of nth CS is expressed as

$$L(n) = L' - \left[T - \sum_{i=1}^{n} t_{\text{cap}}(i) \right] v_{\text{A.E.}}(n), \tag{1}$$

where $L(n)$ is the residual length of nth CS compared to the pristine one; L' is the axial etching length of outmost CS; T is total etching time of peeled tubes; $t_{\text{cap}}(i)$ is time consumed in the opening step of nth cap; $v_{\text{A.E.}}(n)$ is the axial etching rate of the nth CS.

The peeling of MWNTs is simplified as a combination of competitive etching from different blocks. The mean etching rate, $\overline{v}_{\text{A.E.}}(B_j)$, is used to present similar $v_{\text{A.E.}}(i)$ in the B_j. The mean opening time, $\overline{t}_{\text{cap}}$, is used to present similar opening of end-cap in the B. We therefore extend Eq. (1) to the etching of jth B after SCW oxidation and expressed as

$$L(B_j) = L' - \left[T - \overline{t}_{\text{cap}} \sum_{k=1} N_k \right] \overline{v}_{\text{A.E.}}(B_j), \tag{2}$$

where $L(B_j)$ is the residual length in the jth B. N_k is the total number of end-cap in each B. Two adjoining blocks are designated as B_j and B_{j+1} with corresponding mean etching rates $\overline{v}_{\text{A.E.}}(B_j)$ and $\overline{v}_{\text{A.E.}}(B_{j+1})$, respectively. The difference of residual length between two adjoining blocks is $L(B_{j+1}) - L(B_j)$ and expressed as

$$L(B_{j+1}) - L(B_j) = -T\overline{v}_{\text{A.E.}}(B_{j+1}) + \overline{t}_{\text{cap}}\overline{v}_{\text{A.E.}}(B_{j+1}) \sum_{k=1}^{j+1} N_k + T\overline{v}_{\text{A.E.}}(B_j) - \overline{t}_{\text{cap}}\overline{v}_{\text{A.E.}}(B_j) \sum_{k=1}^{j} N_k. \tag{3}$$

Equation (3) is generalized further into Eq. (4) and expressed as

$$\Delta L = \left(T - \overline{t}_{\text{cap}} \sum_{k=1}^{j} N_k \right) \Delta\overline{v}_{\text{A.E.}} + N_{j+1}\overline{t}_{\text{cap}}\overline{v}_{\text{A.E.}}(B_{j+1}), \tag{4}$$

where $\Delta L = L(B_{j+1}) - L(B_j)$ and $\Delta\overline{v}_{\text{A.E.}} = \overline{v}_{\text{A.E.}}(B_j) - \overline{v}_{\text{A.E.}}(B_{j+1})$. Equation (4) shows that the sign of ΔL depends only on $\Delta\overline{v}_{\text{A.E.}}$, since the other terms are positive. From theoretical calculations,[21] we expect stronger adsorption of H_2O and O_2 molecules on zigzag than at armchair edge. Chemisorption occurs preferentially on zigzag tube edges of MWNTs with coaxial CSs containing both armchair and zigzag nanotubes when exposed to SCW and O_2 molecules. The oxidized nanotubes undergo successive transformation into stable geometry with broken C–C bonds.[22]

There are three combinations that will vary the morphology of MWNTs in SCW oxidation. They are: (I) $\overline{v}_{\text{A.E.}}(B_j) \sim \overline{v}_{\text{A.E.}}(B_{j+1})$, (II) $\overline{v}_{\text{A.E.}}(B_j) > \overline{v}_{\text{A.E.}}(B_{j+1})$, and (III) $\overline{v}_{\text{A.E.}}(B_j) < \overline{v}_{\text{A.E.}}(B_{j+1})$. In case I, MWNTs consist of a series of similar iso-etching blocks and possess similar axial etching rate. There are no noticeable divergences in the axial etching rates between adjoining blocks. Only a slight difference in residual lengths between coaxial CSs is expected, which is due to the difference in initial end-cap stripping. A series of approximate axial etching of blocks cause quasiconical shapes with gentle incline contour [Fig. 1(a)]. In our experiments, we seldom observed peeled tubes with gentle incline contour. In case II, the outer B_j possesses larger $\overline{v}_{\text{A.E.}}(B_j)$, which leads to the formation of trapezoid contour between B_j and B_{j+1}. We observed trapezoid contour frequently in our experiments [Figs. 1(b) and 1(c)]. In case III, the inner B_{j+1} is more susceptible to SCW oxidation than the outer B_j, which would delay the end-cap being stripped-off and generates flat step etched edge in peeled tubes, presumably due to parallel etching rate, as shown in Fig. 1(d) and our previous results.[15] Furthermore, case III may cause concave contour of peeled tubes due to the enormous negative remainder of mean etching rate, which we did not observe. This is presumably due to the outer CSs prohibiting the inner shells from reacting with the oxidants and slowing the axial etching rate of inner CSs while $L(B_{j+1})$ is close to $L(B_j)$. When particularly severe conditions (increasing reaction time and amounts of oxygen) are used in SCW oxidation, several etched sites appear in the tube [Fig. 1(e)]. The result implies that there are more peeled tubes with different B. They could be readily observed and distinguished if adequate oxidative condition is applied.

The low-loss EELS spectra along the longitude axis of peeled tubes are obtained, which provide additional information about the electronic structure. Figure 3(a) shows EELS spectra in an energy region from 0 to 50 eV obtained from the peeled sites to unpeeled sites along the longitude axis of tube in Fig. 3(b). The unpeeled sites of tubes [indicated as c and d in Fig. 3(b)] show two distinct plasmon responses, with the π electrons responding at $\sim$7 eV and the $\pi+\sigma$ at $\sim$26 eV (arrows). As the number of shells in the same peeled tube reduces [indicated as b and a in Fig. 3(a)], the $\pi+\sigma$ peak shifts to lower energy loss. Ajayan *et al.*[18] have shown similar results that the energy loss of $\pi+\sigma$ plasmon peak decreases with reducing diameter and decreasing number of shells in different MWNTs. Spectrum b in Fig. 3(a) shows a weak shoulder at $\sim$13 eV in the "turning sites" from peeled to unpeeled sites of tube. Interpretations of the 13 eV peak range from curvature effects to intershell interactions to the

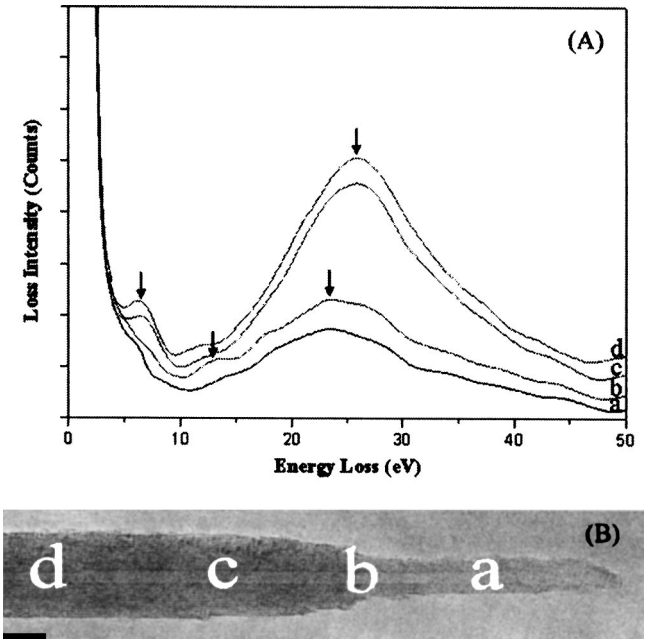

FIG. 3. (a) EELS spectra of peeled-tube taken from image of (b) indicated at a, b, c, and d sites. (b) TEM images of peeled tube in SCW oxidation at 27.5 MPa, 60 min, 400 °C, and ~2 mmol O_2.

presence of amorphous carbon. Nevertheless, disorder of dangling bonds and curvature effect in the "turning site" of peeled tube may result at the 13 eV surface plasmon peak.[23]

A concept of intrinsic character of each CS dominating the etching rate and a simplified etching model is proposed to explain the morphological variation of MWNTs in SCW oxidation. The difference in mean etching rate between two adjoining blocks causes the morphological variation. The EELS results show that the characteristic energy-loss peaks are changed as a function of total shell numbers along longitude axis of individual peeled tube. The potential use of EELS spectra to further understand the electron interactions of "turning sites" in peeled tubes as scanning probes and electron emitters is promising.

Financial support by the National Science Council of the Republic of China under Grant No. NSC92-2113-M007-058 is gratefully acknowledged.

[1]S. Iijima, Nature (London) **354**, 56 (1991).
[2]S. Iijima and T. Ichihashi, Nature (London) **363**, 603 (1993).
[3]J. Cumings, P. G. Collins, and A. Zettl, Nature (London) **406**, 586 (2000).
[4]P. G. Collins, M. S. Arnold, and P. Avouris, Science **292**, 706 (2001).
[5]X. Y. Zhu, S. M. Lee, Y. H. Lee, and T. Frauenheim, Phys. Rev. Lett. **85**, 2757 (2000).
[6]P. W. Ajayan, T. W. Ebbesen, T. Ichihashi, S. Iijima, K. Tanigaki, and H. Hiura, Nature (London) **362**, 522 (1993).
[7]C. H. Kiang, J. S. Choi, T. T. Tran, and A. D. Bacher, J. Phys. Chem. B **103**, 7449 (1999).
[8]S. C. Tsang, P. J. F. Harris, and M. L. H. Green, Nature (London) **362**, 520 (1993).
[9]S. C. Tsang, Y. K. Chen, P. J. F. Harris, and M. L. H. Green, Nature (London) **372**, 159 (1994).
[10]S. H. Tsai, C. W. Chao, L. C. Lee, and H. C. Shih, Appl. Phys. Lett. **74**, 3462 (1999).
[11]C. Y. Zhi, X. D. Bai, and E. G. Wang, Appl. Phys. Lett. **81**, 1690 (2002).
[12]H. H. Yang and C. A. Eckert, Ind. Eng. Chem. Res. **27**, 2009 (1988).
[13]P. E. Savage, Chem. Rev. (Washington, D.C.) **99**, 603 (1999).
[14]M. J. Antal, M. Carlsson, X. Xu, and D. G. M. Anderson, Ind. Eng. Chem. Res. **37**, 3820 (1998).
[15]J. Y. Chang, A. Ghule, J. J. Chang, S. H. Tzing, and Y. C. Ling, Chem. Phys. Lett. **363**, 583 (2002).
[16]J. Y. Chang, F. D. Mai, B. Lo, J. J. Chang, S. H. Tzing, A. Ghule, and Y. C. Ling, Chem. Commun. (Cambridge) **2003**, 2362.
[17]V. P. Dravid, X. Lin, Y. Wang, X. K. Wang, A. Yee, J. B. Ketterson, and R. P. H. Chang, Science **259**, 1601 (1993).
[18]P. M. Ajyan, S. Ijima, and T. Ichihashi, Phys. Rev. B **47**, 6859 (1993).
[19]R. Kuzuo, M. Terauchi, and M. Tanaka, Jpn. J. Appl. Phys., Part 2 **31**, L1484 (1992).
[20]T. W. Ebbesen and P. M. Ajayan, Nature (London) **358**, 220 (1992).
[21]C. Kim, Y. S. Choi, S. M. Lee, J. T. Park, B. Kim, and Y. H. Lee, J. Am. Chem. Soc. **124**, 9906 (2002).
[22]C. Y. Moon, Y. S. Kim, E. C. Lee, Y. G. Jin, and K. J. Chang, Phys. Rev. B **65**, 155401 (2002).
[23]L. A. Bursill, P. A. Stadelmann, J. L. Peng, and S. Prawer, Phys. Rev. B **49**, 2882 (1994).